Estimation of the strain field from full-field displacement noisy data

Comparing finite elements global least squares and polynomial diffuse approximation

Stéphane Avril* — Pierre Feissel — Fabrice Pierron***
Pierre Villon**

** Laboratoire de Mécanique et Procédés de Fabrication*
Ecole Nationale Supérieure d'Arts et Métiers
BP 508 rue Saint Dominique
F-51006 Châlons en Champagne

*** Laboratoire Roberval de Mécanique, UTC*
BP 20529 rue Personne de Roberval
F-60205 Compiègne

ABSTRACT. *In this study, the issue of reconstructing strain fields from corrupted full-field displacement data is addressed. Two approaches are proposed, a global one based on Finite Element Approximation (FEA) and a local one based on Diffuse Approximation (DA). Both approaches are compared on a case study which is supposed difficult (open-hole tensile test). DA provides more stable results, but is more CPU time consuming. Eventually, it is proposed to monitor locally the filtering effect of both approaches, the prospects being an impending improvement of the reconstruction for both approaches.*

RÉSUMÉ. *Cette étude s'intéresse à la reconstruction de champs de déformation à partir de mesures de champs de déplacements bruités. Deux approches sont étudiées : l'une globale s'appuyant sur des approximations éléments finis (AEF) et l'autre locale s'appuyant sur l'approximation diffuse (AD). Ces deux approches sont comparées sur un cas test considéré comme difficile (essai de traction sur éprouvette trouée). L'AD donne des résultats plus stables, mais coûte plus cher en temps de calcul. Finalement, un contrôle localisé de l'effet de filtrage des deux approches est proposé en perspective pour une amélioration prochaine de la reconstruction.*

KEYWORDS: *full-field measurements, numerical differentiation, measurement uncertainty.*

MOTS-CLÉS : *mesures de champs, dérivation numérique, incertitude de mesure, identification.*

DOI:10.3166/REMN.17.857-868 © 2008 Lavoisier, Paris

1. Introduction

The recent development of digitized full-field displacement measurements opens new ways of characterizing materials in solid mechanics (Kobayashi, 1993). However, for most of the users of these techniques the strain fields rather than the displacement fields provide a real insight into the physics of the material at different scales. Therefore, except for the techniques which provide directly the displacement derivatives, it is necessary to differentiate the data. When the gradients of the displacement fields are relatively low, for example when the materials still behave elastically, the small measurement errors may induce large errors on the computed derivative (Geers *et al.*, 1996). So the key work is to develop a stable algorithm, in which it is possible to quantify explicitly the effects induced by noise differentiation.

A large number of algorithms can be found in the literature. A survey of these methods is briefly presented in (Wei *et al.*, 2006). The most common approach is the finite difference method (Wei *et al.*, 2006). Simple and effective with precise data, it is implemented in most of the softwares providing full-field displacement data. However, when the level of noise is significant, filtering is required.

One widely used way of performing this filtering consists in interpolating or approximating the data using smooth basis functions. The differentiation of the data is turned into the differentiation of the basis functions. For a given basis of functions, the regularization parameter is tied to the number of functions used in the basis. A good compromise between the faithfulness of the reconstruction (obtained with a large number of basis functions) and the efficiency of the low pass filtering (obtained with a small number of basis functions) has to be found.

However, a good choice of the basis functions is essential (Hickernell *et al.*, 1999). The approximation can be defined either globally (Lira *et al.*, 2004), or locally (Cleveland *et al.*, 1995). Previous studies (Pierron *et al.*, 2007) showed that a global polynomial basis leads to parasitic oscillations in the reconstruction when the degree of the polynomials is too large. Indeed, because of the global aspect of this type of bases, local artifacts in the data affect the whole reconstruction. Accordingly, it seems that basis functions that have limited interactions between each other would be more appropriate.

Two approaches fulfilling this requirement have been chosen and this paper is aimed at comparing them. The first approach is based on global least-squares minimization using Finite-Element shape functions as the basis functions (FEA) (Feng *et al.*, 1991). The second approach is based on local weighted least-squares minimization using a polynomial diffuse approximation (DA) (Nayroles *et al.*, 1991). The regularization/precision parameter is the mesh size for the first approach, the span of the weighting function in the second one.

In a first section, the framework and the principle of the proposed approaches are presented. Then, their efficiency is compared using simulated data. Eventually, the approaches are applied onto real data for solving a problem of damage detection.

2. Framework and presentation of the approaches

2.1. *Framework and notations*

The proposed approaches are aimed at deriving strain fields from a set of full-field displacement measurements. These measurements are derived from the deformation of a pattern bonded onto the investigated solid, for instance using digital image correlation (Schreier *et al.*, 2002) or fringe analysis (Surrel, 1994). Let us consider a given zone Ω. The input data for deriving strain fields across Ω are therefore the displacements in both directions given at the nodes (called pixels) of a regular grid, whose coordinates are denoted $\underline{x}_i$. In the proposed examples, this grid is made of $N = 168 \times 224$ pixels. These measurements are denoted as:

$$\underline{\tilde{u}}(\underline{x}_i) = \underline{u}_{ex}(\underline{x}_i) + \delta\underline{u}(\underline{x}_i) \quad , \forall i \in [1,N] \qquad [1]$$

where $\delta\underline{u}$ represents the measurement error and $\underline{u}_{ex}$ is the exact mechanical field. The objective is to derive the gradients of $\underline{u}_{ex}$ to obtain the exact strains.

In the following sections, the data are simulated or measured onto a plate tested in an open-hole tensile configuration, which is a difficult case with large strains concentrated near the hole (Balaco de Morais, 2000). The simulated data are obtained with a reference calculation (numerical example) in order to evaluate properly the reconstruction errors. The measured data are obtained on a real test carried out onto a glass/epoxy composite laminate. In the case of simulated data, $\underline{u}_{ex}$ and $\delta\underline{u}$ are known.

Since the reconstruction operator is linear (see 3.2), the reconstructed field $\underline{u}_{ap}(\underline{x})$, at any $\underline{x}$, can be split up into three parts as follows:

$$\underline{u}_{ap}(\underline{x}) = \underline{u}_{ex}(\underline{x}) + \delta\underline{u}_k(\underline{x}) + \delta\underline{u}_b(\underline{x}) \qquad [2]$$

where $\delta\underline{u}_k(\underline{x})$ corresponds to the error due to the approximation of the exact field and $\delta\underline{u}_b(\underline{x})$ is the error due to the noise contained in the measurements.

Due to the linearity of the differentiation operator, the reconstructed strains can be similarly split up in three terms.

2.2. *First approach: global least squares/finite element approximation*

A first group of methods consists in using global least-squares minimization over the whole measurement zone Ω. The choice of the basis functions on which the measurements will be projected will affect the regularity and the precision of the reconstruction. FEA (Feng *et al.*, 1991), where the basis functions only have very low interactions between each other, is chosen in this study because it limits reconstruction oscillations as the precision increases, contrarily to polynomial basis functions (Pierron *et al.*, 2007). The regularization parameter is hence the mesh size of the FEA.

The reconstructed displacement field is written like this:

$$u_{ap}(\underline{x}) = [\Phi(\underline{x})]\, U \qquad [3]$$

where $[\Phi(\underline{x})]$ is the matrix of the shape functions and U is the vector of the nodal displacements. In our examples, the elements are triangles with linear shape functions.

U is found as the solution of the following minimization:

$$\min_U \sum_{i=1}^{N} (u_{ap}(\underline{x}_i) - \tilde{u}(\underline{x}_i))^2 \qquad [4]$$

The minimization problem [4] leads to a linear system to be solved, yielding U.

The strain field is directly derived from $u_{ap}(\underline{x})$, by differentiating the shape functions. In order to keep an approximated strain field described with the same shape functions, $\varepsilon_{ap}(\underline{x}) = [\Phi(\underline{x})]\, E$, with E the nodal strains, the strain field is projected onto the same basis of functions. Its nodal values E are the solution of the following global least-squares problem:

$$\min_E \int_\Omega (\varepsilon_{ap}(\underline{x}) - [B(\underline{x})]\, U)^2 \, dS \qquad [5]$$

where $[B(\underline{x})]$ is the symmetric gradient of $[\Phi(\underline{x})]$.

2.3. *Second approach: diffuse approximation/polynomial approximation*

A second group of methods is based on the use of local regression (Cleveland *et al.*, 1995). Here, DA (Nayroles *et al.*, 1991) is chosen with polynomial basis functions, various degrees being tested. As this approach is based on weighted least-squares, a key point is the span of the weighting function, denoted R. This parameter can be tuned to obtain the best regularization/precision compromise. As presented below, the (diffuse) derivatives are directly derived from the measurements with this approach.

DA enables to define a continuous field from a discrete number of data points. Given $p(\underline{x})$ a vector of basis functions, the starting point is to define, for any $\underline{x}$, the vector of coefficient $\{a(\underline{x})\}$, which will be the solution of a local weighted least-squares across the neighborhood $V(\underline{x})$ of $\underline{x}$:

$$\min_{a(\underline{x})} \frac{1}{2} \sum_{i \in V(\underline{x})} w(\underline{x}, \underline{x}_i) \left(p(\underline{x}_i - \underline{x})^T \{a(\underline{x})\} - \tilde{u}(\underline{x}_i) \right)^2 \qquad [6]$$

$\underline{x}$ being a constant with respect to the minimization and the weighting function $w(\underline{x}, \underline{x}_i)$ being evaluated at each data point. $w(\underline{x}, \underline{x}_i)$ can be any function defined over a bounded domain. The bounded domain requirement is aimed at keeping the local character of the reconstruction. Here, the weighting function is defined as:

$$w(\underline{x}, \underline{x}_i) = w_{ref}(\frac{x - x_i}{R_x}) w_{ref}(\frac{y - y_i}{R_y}) \qquad [7]$$

where w_{ref} is a dimensionless window function whose derivative zeroes at 0 and 1 (this aspect ensures continuity up to the first derivative of the reconstructed fields); here R_x and R_y are chosen independant of $\underline{x}_i$ but may depend on $\underline{x}$.

Then, $\{a(\underline{x})\}$ is a vector field such that, if the basis is composed of monomials up to at least degree 1, the approximate field and its first derivatives are reconstructed as:

$$u_{ap}(\underline{x}) = a_1(\underline{x}), \quad \frac{\delta u_{ap}}{\delta x}(\underline{x}) = a_2(\underline{x}) \quad \text{and} \quad \frac{\delta u_{ap}}{\delta y}(\underline{x}) = a_3(\underline{x}) \qquad [8]$$

where $\frac{\delta u}{\delta x}$ denotes the diffuse derivative which is an approximation of the exact derivative. This reconstruction can be applied to each component of the displacement field $\underline{\tilde{u}}(\underline{x}_i)$. The strain fields can be deduced subsequently from the first order diffuse derivatives. Let us finally mention that this approach implies the resolution of problem [6] at each evaluation point. This means that one has to choose the evaluation points. Here, they are chosen as coincident with the pixels where data are provided. Accordingly, the reconstruction is evaluated through the discrete grid of the points $\underline{x}_i$, $i \in [1,N]$.

3. Understanding and illustrating the methods with a numerical example

3.1. *Numerical data and strain reconstruction*

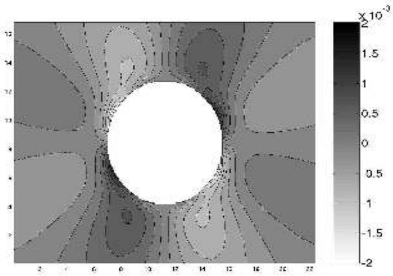

Figure 1. *Exact shear strain field to be reconstructed*

In this section, the two methods presented in Section 2 are applied to simulated data. A FE simulation of the tensile response of an elastic isotropic plate with a hole is thus performed. The obtained displacement field is then used to create a grid of data points and a white noise, with a realistic standard deviation equal to 5% of the maximum displacement, is added in order to represent the perturbation on the measurements. The strain is reconstructed from these measurements. At first, the strain reconstruction is illustrated on the shear strain field ε_{XY}. In order to compare visually the quality of the reconstruction, the exact field is plotted in Figure 1. Figures 2 and 3 show the shear strain field reconstructed by both approaches for two different regularization parameters (mesh size or span of the weighting function) in each case. Let us remark that the larger the mesh size or span of the weighting function, the smoother the results. But the reconstructed field appears smoother with DA since the FEA first derivative is only C^0 at the edges of the elements, rending almost visible the mesh. In both cases, the approximation error $\delta\varepsilon_k$ remains quite small and is smaller in the DA approach. This will be confirmed in Section 4.1.

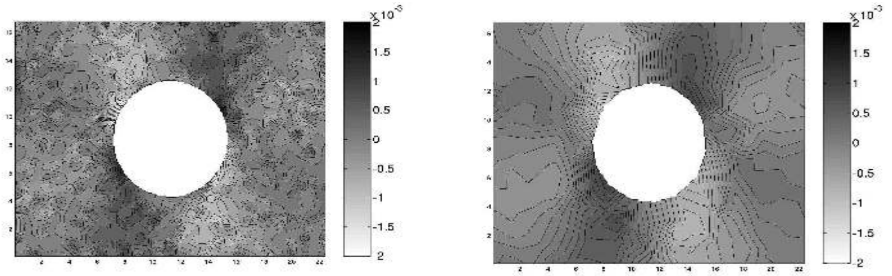

(a) Mesh size : $h = 5 pixels$ (b) Mesh size : $h = 12 pixels$

Figure 2. *Reconstructed shear strain field* ε_{XY} *with the FEA approach*

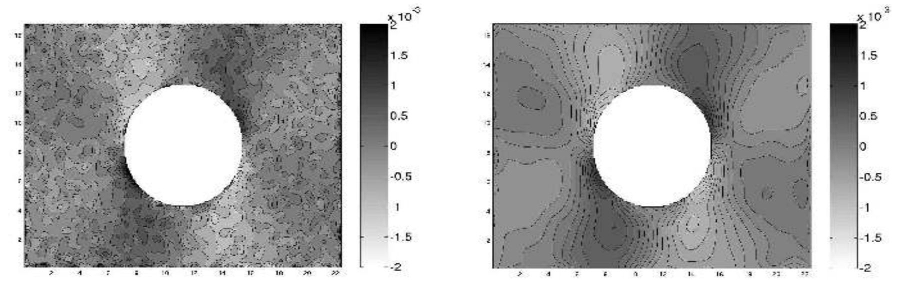

(a) Weight span $R = 7 pixels$ (b) Weight span $R = 18 pixels$

Figure 3. *Reconstructed shear strain field* ε_{XY} *with the DA method*

3.2. *Reconstructing operator*

As explained in Section 2, the two proposed methods lead to the resolution of linear problems, which means that the reconstruction operators are linear. The first consequence is that, in the additive decomposition [2], the $\delta\underline{u}_b$ term corresponds to the reconstruction of the noise alone and the $\delta\underline{u}_k$ term is related to the reconstruction of the exact field. One can therefore study them separately. The second point is that one can define the Green's functions of the reconstructing operator. The Green's function at point $\underline{x}_i$ can be obtained as the reconstructed field with measurements such as: $\tilde{u}(\underline{x}_j) = \delta_{ij}$, with δ_{ij} the Kronecker function. As shown in Figure 4, the Green's functions confirm that both approaches only have a local domain of influence. In the FEA case, the effect of the mesh is visible.

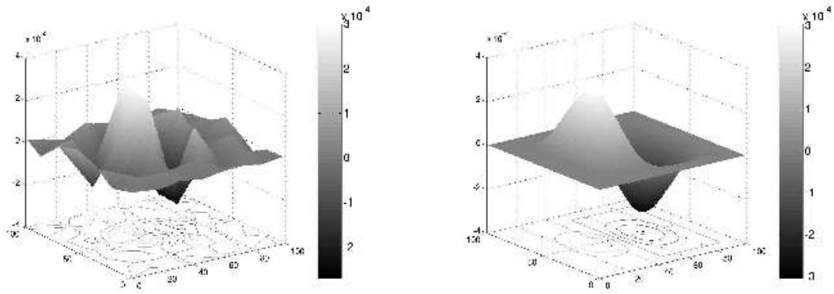

(a) Finite Elements method (b) Diffuse Approximation method

Figure 4. *Green's function of the first order derivative reconstruction operator*

4. Numerical comparison of the methods

The comparison proposed in this section are based on the displacement fields obtained from a simulation and described in Section 3.1.

4.1. *Global reconstruction error*

In this section, we propose to compare the two reconstruction approaches from a quantitative point of view. Consequently, one has to choose a criterium for evaluating the quality of the reconstruction. Since the reconstruction is applied to simulated data, this criterium is defined as a quadratic distance between the reconstructed strain field and the exact one:

$$e_\varepsilon = \left\langle \sqrt{(\varepsilon_{XX}^{ap} - \varepsilon_{XX}^{ex})^2 + 2\,(\varepsilon_{XY}^{ap} - \varepsilon_{XY}^{ex})^2 + (\varepsilon_{YY}^{ap} - \varepsilon_{YY}^{ex})^2} \right\rangle_{\Omega_m} \quad [9]$$

where $\langle \bullet \rangle_{\Omega_m}$ is the average of the data over region Ω_m. Ω_m can be either the whole measurement zone Ω or a smaller zone around the hole where large gradients occur. In Figure 5, error [9] is compared in various cases, for noisy and noiseless data, from strain fields reconstructed with the FEA and the DA approaches. For the latter, the effect of the degree of the polynomial basis, ranging from 1 to 3, has also been studied. As expected, the perturbation error decreases as the mesh size or span of the weighting function increases, whereas the approximation error increases. One can notice that the FEA approach has a larger filtering effect than DA, but induces larger approximation errors, even when the basis functions of DA are of the same degree (degree 1). This can be explained by the larger size of the domain of influence of the FEA reconstruction operator.

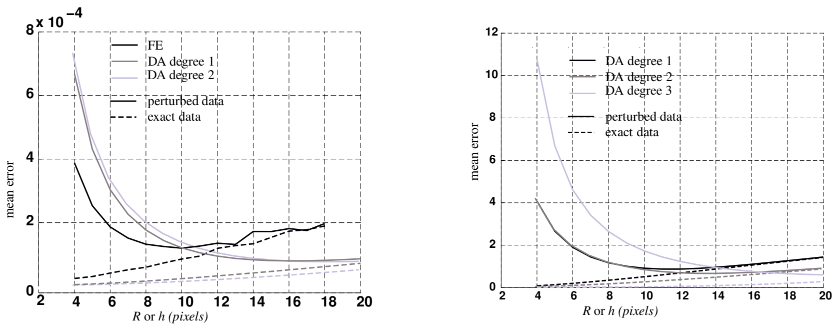

(a) Global error e_{ε} (b) Error e_{ε} near the hole

Figure 5. *Reconstruction error with respect to the characteristic size*

In the considered example, the average of the approximation error obtained with DA remains small. The error at the vicinity of the hole for various degrees of the function basis used in DA is shown in Figure 5(b). One observes that the approximation decreases as the degree increases, and the perturbation error increases. Nevertheless, degree 2 in our case is a good trade off between the filtering effect and the faithfulness of the reconstruction. From the curves plotted in Figure 5(b), it should also be emphasized that the approximation error depends on the zone. Therefore, it would be interesting to use mesh sizes or spans of the weighting function that vary spatially, depending on the zones. In order to do that, one has to define a criterium controlling the local mesh sizes or spans of the weighting function, for example a criterion based on the signal to noise ratio. The implementation of this feature is currently on-going.

4.2. *VFM-based stiffness identification using the reconstructed strains*

According to the basic equations of the Virtual Fields Method (VFM) (Grédiac *et al.*, 2006), the Poisson's ratio of the material should verify the following equation:

$$\nu = -\frac{\displaystyle\int_{\Omega}(\varepsilon_{xx}\varepsilon^*_{xx} + \varepsilon_{yy}\varepsilon^*_{yy} + 2\varepsilon_{xy}\varepsilon^*_{xy})dS}{\displaystyle\int_{\Omega}(\varepsilon_{xx}\varepsilon^*_{yy} + \varepsilon_{yy}\varepsilon^*_{xx} - 2\varepsilon_{xy}\varepsilon^*_{xy})dS} \qquad [10]$$

where ε^* is the strain field derived from a virtual displacement field $\underline{u}^*$ chosen across Ω in such a way that $u^* = 0$ on $\partial\Omega$. The components ε_{xx}, ε_{yy} and ε_{xy} are the experimental strain fields reconstructed from the data. Because of data corruption, equation [10] is not satisfied in practice. Errors exist, but they can be minimized by choosing an optimal virtual field, denoted $\underline{u}^{**}$, according to the principles presented in (Avril *et al.*, 2007).

When ε^{**} is used instead of ε^* in equation [10], the remaining error can be used to quantify the quality of the experimental strain reconstruction from the data. The reference value for ν here is 0.286.

The obtained values of ν for different types of reconstruction (FEA with different mesh sizes, DA with different spans of the weighting function), using noiseless data, are shown in Figure 6(a). It can be noticed that:

– the error increases when the mesh size or the span of the weighting function increases, due to the degrading faithfulness of the reconstruction;

– the curve for DA is smoother than the curve for FEA. Indeed, for a given span of the weighting function, the reconstruction obtained with DA is unique, and so is the identified Poisson's ratio. But for FEA, as many different meshes give as many different reconstructions, hence as many identified Poisson's ratio. This is why the curve for FEA in Figure 6(a) has this serrated aspect.

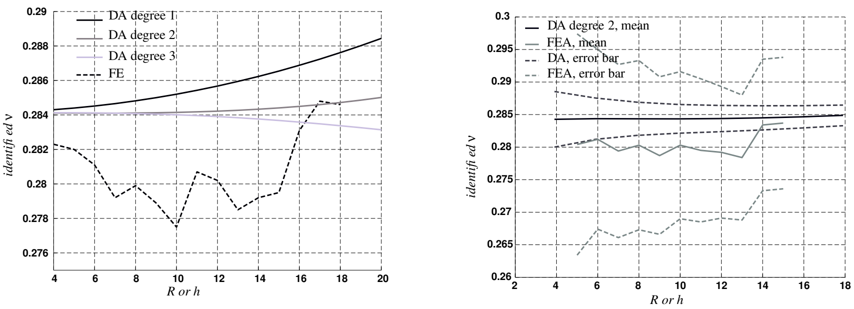

(a) noiseless measurements (b) noisy data - mean value and error bar

Figure 6. *Identified* ν *as a function of the characteristic size*

Identification results obtained with noisy data deduced from the use of 150 samples of white noise are shown in Figure 6(b). It shows the mean value of the identified Poisson's ratio and the error bar of plus and minus the standard deviation. The average of the identified Poisson's ratio on the samples converges to the noiseless case with the number of samples. First, one can remark that the larger the mesh size or the span of the weighting function, the smaller the standard deviation. For DA, the systematic error illustrated on Figure 6(a) remains small with respect to the standard deviation and therefore the increase of the span of the weighting function improves the identification accuracy within the studied range. Furthermore, when using the FEA, the scatter on the identification results is both due to the noise on the measurements and the dependency of the reconstructed field to the mesh (for a given mesh size, two meshes yields two different fields). Since the identification error remains small, the scattering due to the mesh is emphasized and it is not possible to see if a larger mesh size improves the identification results.

Eventually, due to the averaging effect of integration in equation [10], it can be concluded that the error on the Poisson's ratio identified with the VFM does not constitute a relevant criterion for qualifying the reconstruction approaches. Other criteria based on local errors may be used instead.

5. Real test data: detection of non-linearities

In this section, the two reconstruction approaches are applied to data obtained from an open-hole tensile test carried out onto a glass/epoxy laminated plate having a quasi-isotropic stacking sequence: $[-45_4, 90_4, 45_4, 0_4]_s$. In such tests, fracture of the 90° underlying plies occurs quite early. An objective of full-field displacement fields is to detect the onset and spatial location of this fracture. Thirty snapshots of the displacement fields were measured with the grid method (Surrel, 1994) in a region around the hole of the specimen, for tensile loads ranging from 0 to $13.3\,kN$. It has been proposed in (Pierron *et al.*, 2007) to characterize the fracture process by detecting local non linearities of the response. A first estimation of these non-linearities is obtained by computing the discrepancy between the real strain field and the strain field resulting from the extrapolation of the linear response. One has therefore to determine the latter.

The linear response is estimated from the first ten snapshots, $i \in \{1,..10\}$, F_i being the corresponding load , as the slope of the response of each pixel:

$$\min_{\varepsilon_{lin}} \sum_{i}^{N_{lin}} \left(F_i \varepsilon_{lin} - \varepsilon(\underline{x}, F_i)\right)^2 \quad \text{with,} \quad N_{lin} = 10 \qquad [11]$$

Then, it is possible to define the non-linear part of the strain field for a given load F:

$$\Delta\varepsilon(\underline{x}, F) = F\varepsilon_{lin}(\underline{x}) - \varepsilon(\underline{x}, F) \qquad [12]$$

The $\Delta\varepsilon$ fields reconstructed by the two approaches are shown for two different loads in Figure 7. The detection of the non-linearities around the hole gives better results than the previous method used in (Pierron *et al.*, 2007), with a sharper zone providing a more precise localization. Both methods yield similar results, even if the FEA approach remains sensitive to the underlying mesh. The DA is more affected by the noise differenciation but seems to offer a better contrast. Nevertheless, the perturbations on the measurements are more severe than in the numerical case and one would have to input more *a priori* information on the fields to get better results. This suggests considering regularization approaches, which are considered as one of the major prospects of this study.

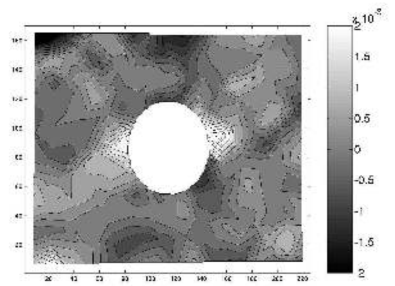

(a) Load 9.7 kN - FEA

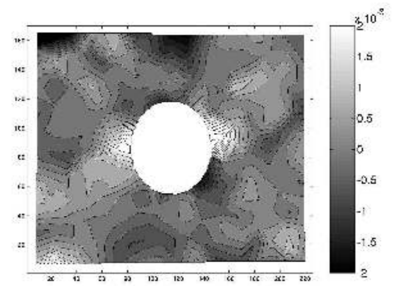

(b) Load 13.3 kN- FEA

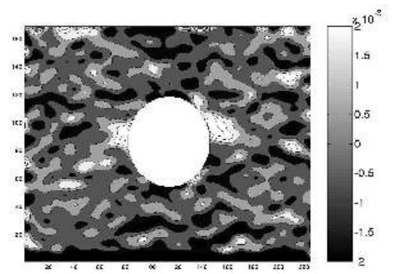

(c) Load 9.7 kN - DA

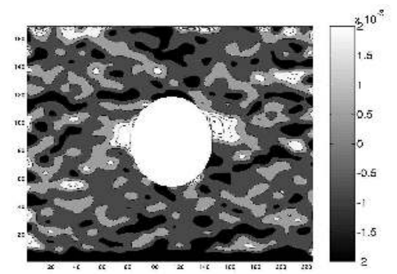

(d) Load 13.3 kN - DA

Figure 7. *Non-linear part of the displacement from the reconstructed fields*

6. Conclusion

This paper has presented two methods for reconstructing strain fields from full-field displacement data. The aim of the methods is to handle measurement perturbations and control their filtering. In both methods, the regularization and the precision of the reconstructed fields are controlled by only one parameter, the mesh size or the span of the weighting function. The results on the examples are satisfactory. The FEA approach has a lower computational cost, but provides larger errors in the reconstructed field. Another disadvantage is the dependency of the approximation to the mesh, even for a given mesh size, yielding less robust results. The DA approach does not have this drawback and offers a richer way of reconstructing the fields, by making easier the choice of parameters controlling the errors. Furthermore, the DA approach enables the enrichment of the basis by any function, further work should be devoted to the introduction of some mechanical knowledge through mechanical fields in the basis.

It has been shown on a first example that the choice of the mesh size (FEA) or the span of the weighting function (DA) can improve the reconstruction quality. Therefore, it would be interesting to establish a criterion for choosing them as point dependent functions, leading to size maps for the reconstruction process. Studies about the choice of a relevant criterion are still on-going.

Finally, once the choice of the parameters controlling the errors is optimized in both approaches, implementation of regularization techniques, such as Tikhonov ones, will be investigated for further improvements.

7. References

Avril S., Pierron F., " General framework for the identifi cation of constitutive parameters from full-field measurements in linear elasticity", *International Journal of Solids and Structures*, vol. 44, p. 4978-5002, 2007.

Balaco de Morais A., " Open hole tensile strength of quasi-isotropic laminates", *Composites Science and Technology*, vol. 60, p. 1997-2004, 2000.

Cleveland W., Loader C., *Smoothing by local regression: principles and methods*, Springer, 1995.

Feng Z., Rowlands R., " Smoothing fi nite-element and experimental hybrid technique for stress analyzing composites", *Computers and Structures*, vol. 6, p. 631-639, 1991.

Geers M., De Borst R., Brekelmans W., " Computing strain fields from discrete displacement fields in 2D solids", *International Journal of Solids and Structures*, vol. 33, n° 29, p. 4293-4207, 1996.

Grédiac M., Pierron F., Avril S., Toussaint E., " The virtual fields method for extracting constitutive parameters from full-field measurements: a review", *Strain*, vol. 42, p. 233-253, 2006.

Hickernell F. J., Hon Y. C., " Radial basis function approximations as smoothing splines", *Applied Mathematics and Computation*, vol. 102, n° 1, p. 1-24, 1999.

Kobayashi A., *Handbook on Experimental Mechanics*, Wiley, 1993.

Lira I., Cordero R., François M., Vial-Edwards C., " The uncertainty of experimental derivarives: application to strain measurement", *Measurement Science and technology*, vol. 15, p. 2381-2388, 2004.

Nayroles B., Touzot G., Villon P., " La méthode des éléments diffus", *Comptes rendus de l'Académie des Sciences, série 2, Mécanique, Physique, Chimie, Sciences de l'Univers, Sciences de la Terre*, vol. 313, n° 2, p. 133-138, 1991.

Pierron F., Green B., Wisnom M. R., " Full-field assessment of the damage process of laminated composite open-hole tensile specimens. Part I: Methodology", *Composites Part A: Applied Science and Manufacturing*, 2007.

Schreier H., Sutton M., " Systematic errors in digital image correlation due to undermatched subset shape functions", *Experimental Mechanics*, vol. 42, p. 303-310, 2002.

Surrel Y., " Moiré and grid methods: a signal processing approach.", *in* J. Pryputniewicz, Ryszard J. et Stupnicki (ed.), *Interferometry '94: Photomechanics*, vol. 2342, The International Society for Optical Engineering, SPIE, p. 213-220, Nov, 1994.

Wei T., Li M., " High order numerical derivatives for one-dimensional scattered noisy data", *Applied Mathematics and Computation*, vol. 175, p. 1744-1759, 2006.